Structure and transport properties of a porous magnetic gel via x-ray microtomography

M. D. Rintoul,[1,2] S. Torquato,[1,2] C. Yeong,[1,2] D. T. Keane,[3] S. Erramilli,[2,4] Y. N. Jun,[2,4] D. M. Dabbs,[2,5] and I. A. Aksay[2,5]

[1]*Department of Civil Engineering and Operations Research, Princeton University, Princeton, New Jersey 08544*

[2]*Princeton Materials Institute, Princeton University, Princeton, New Jersey 08540-5211*

[3]*DuPont-Northwestern-Dow Collaborative Access Team Synchrotron Research Center, Argonne National Laboratory, Argonne, Illinois 60439*

[4]*Department of Physics, Princeton University, Princeton, New Jersey 08544*

[5]*Department of Chemical Engineering, Princeton University, Princeton, New Jersey 08544*

(Received 13 March 1996)

A three-dimensional digitized image of a porous magnetic gel is determined by x-ray microtomographic techniques. The complex connected pore-space topology is quantitatively characterized by measuring a variety of statistical correlation functions, including the chord-length distribution function, the pore-size distribution function, and the lineal-path function. This structural information is then employed to estimate transport properties, such as the fluid permeability and trapping rate, of the gel. [S1063-651X(96)06408-2]

PACS number(s): 61.20.−p, 05.20.−y

I. INTRODUCTION

Two-phase random media, such as composite materials, dispersions, and porous media, are of great technological importance. The transport and mechanical properties of such a random material depend on an infinite set of n-point correlation functions that statistically characterize the structure [1–3]. Generally, such complete morphological information is not available. However, by using only the lower-order correlation function information, one can obtain rigorous bounds on many of the properties of the random materials [1–10], which are often very sharp and their use is limited only by one's ability to extract the lower-order correlation functions for the random materials. The preponderance of such work has been carried out for theoretical model microstructures.

It has recently become possible to obtain two- and three-dimensional microstructural phase information using a variety of experimental techniques. Such techniques include transmission microscopy [11], scanning tunneling electron microscopy [12], synchrotron-based tomography [13], and confocal microscopy [14]. These techniques have the advantage of giving high-resolution images and being nondestructive, allowing results to be checked by other means. Recently, microtomographic methods in particular have been used to study the structure and properties of sandstones [15,16].

In this paper we analyze a three-dimensional digitized image of a magnetic gel obtained via x-ray microtomographic techniques. This sample is ideally suited for a tomographic analysis since it is too fragile to be characterized (structurally and for its bulk properties) using standard experimental techniques. The gels were synthesized for the purpose of filtration and separation of labeled rare biological cells [17]. We ascertain a number of different correlation functions, some of which are experimentally obtainable from lineal, plane, and/or volume measurements. The most basic and simplest quantities are the *volume fraction of phase* i, ϕ_i, and *specific surface* (the interfacial surface area per unit volume) s. Higher-order statistical correlation functions are extracted, including quantities that contain the important topological property of connectedness of the phases. A determination of the transport properties of fluids within the porous gels from purely structural measurements would be useful in designing new porous materials that are designed for specific applications. The statistical measures extracted here are crucial in determining a variety of transport and mechanical properties of the gels. It is also advantageous to have a means of determining the transport properties of materials that may be too delicate or too small for standard tests.

The paper is organized as follows. A description of the preparation of the gel sample and x-ray microtomographic techniques is given in Sec. II. The relevant correlation functions and their relationships to physical properties are discussed in Sec. III. In Sec. IV we give the results of the computer analysis of the sample and extract some of the length scales involved in the problem. Section V contains a discussion of the results. Finally, we make concluding remarks in Sec. VI.

II. SAMPLE PREPARATION AND X-RAY TOMOGRAPHY

A. Sample preparation

The preparation of the gel has been described by Jun *et al.* [17]. First, a silica gel was prepared by mixing tetraethoxysilane (TEOS), ethanol, and water in the volumetric proportions 1.5:1:1. The incipient gel was stirred for 24 h using a magnetic stirrer, then mixed with a ferrofluid (product EMG 705, Ferrofluidics) composed of $\approx$100-Å magnetite particles in aqueous suspension. Porosity at the micrometer scale was controlled in the gel by mixing the ferrofluid-TEOS gel with a suspension of monosized polystyrene beads (Duke Scientific), using the method of Sonuparlak and Aksay [18]. Samples of continuous porosity were also obtained by incorporating pyrolizable cellulose fibers in the gel. Addition of the ferrofluid induced gelation in the TEOS solution, but homogeneity was maintained by shaking the mixture until the gel had set. The gel was then cured to form a coherent silica-magnetite-pyrolite composite. Supercritical extraction was used to remove ethanol and water

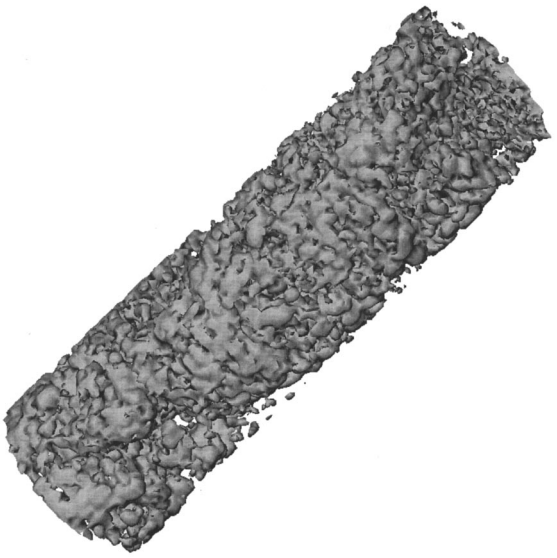

FIG. 1. ''Negative'' of the magnetic gel sample. In this picture, the void is shown as filled to give a better sense of the connectivity of the void structure.

from the gel. The pyrolyzable materials were burned out under air at 300 °C, a process that partially oxidized the magnetite particles. Sintering the gel under dry nitrogen at 700 °C for 3 h both partially sintered the gel, imparting greater structural integrity, and reversed the oxidation of the magnetite particles. Shrinkage during sintering was minimal. A three-dimensional ''negative'' of the resulting gel image is shown in Fig. 1. In this case, the void region is shown as solid in order to present a better picture of the connectedness of the void region.

B. X-ray microtomography

Much early work on the morphology of heterogeneous materials was done via techniques such as sectioning. This approach is unsatisfactory, especially in biomedical applications, not only because it destroys the sample but it also often causes the sections themselves to be altered during the sectioning process. In order to overcome these problems, noninvasive techniques have been developed. CAT scans are a very common way to obtain three-dimensional phase information, especially in the medical field. However, the resolution obtained is approximately ~ 100 μm, so they cannot be used when the length scales of the microstructure of interest are smaller than this.

X-ray microtomography [13,19–21] provides a means to have both high-resolution and nondestructive evaluation of three-dimensional structural information. The microtomography data and reconstructed three-dimensional maps of the gel x-ray opacity were collected using beam line X2B located at the National Synchrotron Light Source of Brookhaven National Laboratory. Beam line X2B was specifically developed for x-ray microtomography experiments by Exxon Research and Engineering [21,22]. White bending magnet radiation (3-mrad divergence) passes through a Be window into the experimental hutch, where it is diffracted in the horizontal plane by a Si(111) monochromator. The samples were scanned with an x-ray beam energy of 17 keV. The monochromatic beam passes through the sample and onto the photo-optic detector. The resolution of the x-ray microtomographic process is typically on the order of a few micrometers and is usually limited by the process in which the transmitted x rays are measured. We used the Exxon detector, a single crystal phosphor imaged by a microscope objective onto a charge coupled device (CCD). The combination of a 4× lens with a 27-μm CCD pixel gives a spatial resolution in the initial images (before reconstruction) of 6.75 μm. Some images were also obtained using a 10× lens, which provides a spatial resolution of 2.75 μm, although these images were not used in this study. The reconstruction of the tomographic images was carried out using direct Fourier inversion, with an algorithm developed by scientists at Exxon Research and Engineering. The resulting data set gives the three-dimensional x-ray opacity of the sample, proportional to the electron density. The reconstruction is done one two-dimensional plane or ''slice'' at a time, with the data for each slice taken by rotating the sample through 180° and storing the ratio of the incident x-ray flux to that transmitted through the sample.

The digitized image of the gel was stored as a $512\times512\times512$ matrix of values, but not all of the voxels contained information, due to the thin, cylindrical shape of the sample. The actual information was contained in a rectangular parallelepiped of voxels whose dimensions were $168\times168\times512$. The values stored in these voxels (which corresponded to the electron densities in the sample) were then binned and the two phases showed up as two peaks in a histogram of the electron density values. Once a cutoff value was determined to distinguish the phases, the sample was stored as a matrix of bits, corresponding to values of either 0 (matrix phase) or 1 (void phase). This resulted in a factor of 16 reduction in size over the original image, which used short integers to store the data instead of bits.

III. STATISTICAL CORRELATION FUNCTIONS

For statistically homogeneous media, the simplest morphological quantities are the porosity ϕ_1 (volume fraction of phase 1) and the specific surface s (interfacial area per unit volume). A commonly employed higher-order correlation function is the so-called two-point probability function $S_2^{(i)}(\mathbf{x}_1,\mathbf{x}_2)$, which gives the probability of finding two points at $\mathbf{x}_1$ and $\mathbf{x}_2$ in phase i [23]. This quantity has been extensively studied theoretically [1,3,4,23] and experimentally [16,24]. It has two undesirable features. First, it is not capable of distinguishing between the separate length scales associated with phase 1 and phase 2 material [1,23]. Second, rigorous bounds on transport properties that depend on $S_2^{(i)}$ [7,8,16] are typically very weak. With additional computational effort, one can obtain three-point versions of this quantity, which often provide useful estimates of the effective conductivities and elastic moduli of composites [1–3].

In light of the above discussion we turn our attention to three other ''two-point'' statistical measures: (i) the *lineal-path function* $L^{(i)}(x)$, (ii) the *chord-length distribution function* $p^{(i)}(x)$, and (iii) the *pore-size distribution function* $P^{(i)}x$. In each of these cases, the superscript i refers to phase i ($i = 1$ or 2), where phase 1 refers to the void phase and phase 2 refers to the solid phase. Each of these functions not

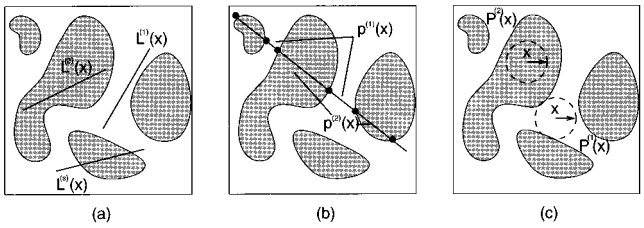

FIG. 2. Graphical description of the statistical correlation functions calculated in this paper: (a) shows the lineal-path function $L(x)$ as defined for both phases, as well as the probability of a line of length x lying in both phases. (b) shows the chords formed by an arbitrary line in the sample. The chords defined this way comprise the chord-length distribution function $p^{(i)}(x)$. Finally, (c) shows how the pore-size distribution $P^{(i)}(x)$ is calculated as the distribution of distances a random point is from the nearest interface.

only can distinguish between phase 1 and phase 2 material but they also contain some information about the *connectedness* of the phases. The three functions are graphically illustrated in Fig. 2.

A. Lineal-path and chord-length functions

Lu and Torquato [25] introduced the so-called *lineal-path function* $L^{(i)}(z)$, which gives the probability of finding a line segment of length wholly contained in phase i. This function is similar to $S_2^{(i)}(r)$ in that it requires two points at a distance r to fall in the same phase, but it also requires all points that lie on a line between them to fall in the same phase. Thus it contains connectedness information *along a lineal path*. There is also a stereological interpretation of $L^{(i)}(x)$: it is the area fraction of phase i measured from the projected image of a three-dimensional slab of thickness z onto a plane. A useful length scale is

$$\lambda_A^{(i)}=\left(\int_0^\infty xL^{(i)}(x)dx\right)^{1/2}, \tag{1}$$

which is just the first moment of $L^{(i)}(x)$. This length scale has been shown to provide a rough measure of average cluster sizes in bicontinuous media [26].

A related morphological measure is the *chord-length distribution function* $p^{(i)}(x)$ [27]. The quantity $p^{(i)}(x)dx$ is the probability of finding a chord of length between x and $x+dx$ lying entirely in phase i. Chords are defined as the segments formed by the intersection of lines with the interface between the two phases. The chord-length distribution function is of importance in fluid transport in porous media [28] and in discrete free-path transport [29,30]. It has been shown by Torquato and Lu [27] that $p^{(i)}(x)$ is related to $L^{(i)}(x)$ by the relation

$$p^{(i)}(x)=\frac{\lambda_C}{\phi_i}\frac{d^2L^{(i)}(x)}{dx^2}, \tag{2}$$

where the length scale λ_C is defined as the first moment of the chord length distribution function

$$\lambda_C^{(i)}=\int_0^\infty xp^{(i)}(x)dz. \tag{3}$$

B. Pore-size distribution function

While the chord-length distribution function can give some notion of the ''length'' of the pores in a porous medium, one can also define a distribution function $P^{(i)}(x)$, which characterizes the ''radius'' of the pores (or material) in phase i. This function is known as the *pore-size distribution function*. It is defined such that $P^{(i)}(x)dx$ is the probability that a randomly chosen point in the phase of interest (usually a void phase) lies at a distance between x and $x+dx$ of the nearest point on the interface between the two phases [10].

Given this definition, we can write down explicitly

$$P^{(i)}(0)=\frac{s}{\phi_i}, \quad P^{(i)}(\infty)=0. \tag{4}$$

The nth moment of this distribution $\langle x^n\rangle$ is defined as

$$\langle x^n\rangle=\int_0^\infty x^nP(x)dx. \tag{5}$$

This allows us to define another length scale λ_D, which is the first moment of the distribution

$$\lambda_D^{(i)}=\langle x\rangle=\int_0^\infty xP^{(i)}(x)dx. \tag{6}$$

The length scale $\lambda_D^{(i)}$ is a measure of the characteristic pore size.

The *cumulative distribution function* $F^{(i)}(x)$ associated with $P^{(i)}(x)$ is defined by

$$F^{(i)}(x)=\int_x^\infty P^{(i)}(z)dz, \tag{7}$$

with

$$F^{(i)}(0)=1, \quad F^{(i)}(\infty)=0. \tag{8}$$

$F^{(i)}(x)$ is the fraction of pore space that has a pore diameter greater than x. This is equivalently the probability that, given a point in the void, one can place a sphere of radius x centered at that point, lying entirely in the void. Thus $F^{(i)}(x)$ and therefore $P^{(i)}(x)$ are intrinsically three-dimensional measures as they provide connectedness information regarding spherical regions of radius x in the medium [31]. Consequently, only three-dimensional imaging techniques, such as tomography or confocal microscopy, can yield such information.

Equation (7) allows us an alternative way to define the moments $\langle x^n\rangle$ as

$$\langle x^n\rangle=n\int_0^\infty x^{n-1}F^{(i)}(x)dx. \tag{9}$$

Specifically, the mean pore size may also be defined in terms of the cumulative pore-size distribution function

$$\lambda_D^{(i)}=\int_0^\infty F^{(i)}(x)dx. \tag{10}$$

C. Analytical expressions for overlapping spheres

An important theoretical model microstructure of heterogeneous media is the overlapping sphere model. In this model, the random medium is constructed by adding identical spatially uncorrelated spheres of radius R to a system to form a two-phase system. Because the spheres overlap, the total volume fraction of the sphere phase, say phase 2, is generally not equal to the sum of the volume fraction of each individual sphere. The porosity and specific surface are given by

$$\phi_1 = e^{-\eta} \tag{11}$$

and

$$s = \frac{3\eta\phi_1}{R}, \tag{12}$$

respectively, where

$$\eta = \rho \frac{4\pi}{3} R^3, \tag{13}$$

η is the reduced density, and ρ is the number density of spheres. It should be noted that while $\phi_2 \leqslant 1$, η can be larger than unity.

The lineal-path function and chord-length distribution for the void phase of a system of overlapping spheres of radius R are given by the expressions [25,27]

$$L^{(1)}(z) = \phi_1^{1+3z/4R} \tag{14}$$

and

$$p^{(1)}(z) = -\frac{3}{4R} \ln(\phi_1)\, \phi_1^{3z/4R}. \tag{15}$$

Substitution of the expression for the chord-length distribution of the overlapping sphere system into Eq. (3) gives the expression for λ_C for that system,

$$\lambda_C^{(1)} = -\frac{4R}{3\ln(\phi_1)}. \tag{16}$$

Finally, the expression for the pore-size distribution in the overlapping-sphere system [10] is

$$P^{(1)}(x) = \frac{3\eta}{\phi_1 R}\left(\frac{x}{R}+1\right)^2 \exp\left[-\eta\left(\frac{x}{R}+1\right)^3\right]. \tag{17}$$

Note that for $x=0$, we just recover the specific surface s, as given in Eq. (12), divided by a factor of ϕ_1.

D. Mean survival time

The mean survival time τ (obtainable from a NMR experiment [32,33]) is the average time a Brownian or diffusing particle takes to diffuse in a trap-free region (with diffusion coefficient D) in a system of partially absorbing traps before becoming absorbed by the trapping phase. Therefore, the quantity $D\tau$ provides an average pore-size measure. Note that the inverse of τ is sometimes referred to as the ''trapping rate.''

The mean survival time τ for perfectly absorbing traps has been rigorously bounded from below in terms of the mean pore size λ_D [10] via the relation

$$\tau \geqslant \lambda_D^2 / D, \tag{18}$$

where D is the diffusion coefficient and λ_D is given by Eq. (6) with $i=1$.

Torquato [34] developed a rigorous cross-property relation that relates the fluid permeability k to the mean survival time τ as

$$k \leqslant \phi_1 D \tau. \tag{19}$$

Thus a measurement of the mean survival time provides an upper bound on the fluid permeability. Relation (19) becomes an equality for transport interior to parallel tubes of arbitrary cross section (in the direction of the tubes). The bound (19) is relatively sharp for flow around dilute arrays of obstacles, e.g., for spheres $k = 2D\phi_1\tau/3$. For a cubic array of narrow tubes it is less sharp: $k = D\phi_1\tau/3$. Generally, inequality (19) is not sharp because τ is a reflection of the entire pore space, whereas k is a reflection of the dynamically connected part of the pore space.

Avellaneda and Torquato [35] derived the rigorous equality connecting the permeability to the effective electrical conductivity σ_e of a porous medium containing a conducting fluid of conductivity σ_1 and an insulating solid phase:

$$k = \frac{L^2}{8F}, \tag{20}$$

where $F = \sigma_1/\sigma_e$ is the formation factor and L is a length parameter that is a weighted sum over the viscous relaxation times associated with the time-dependent Stokes equations.

Since it is difficult to obtain L^2 exactly, rigorous treatments can only provide bounds on L^2. It has been conjectured [36] that for isotropic media possessing an arbitrary but connected pore space, the following relation holds:

$$k \leqslant \frac{D\tau}{F}. \tag{21}$$

Because the right-hand side of (21) appears to overestimate k by roughly a factor of porosity ϕ_1 for a number of porous media, it has been proposed [37] that the approximate relation

$$k \approx \phi_1 \frac{D\tau}{F} \tag{22}$$

should be accurate for a large class of porous media. Recently, it was found that (22) provided a good estimate of the permeability of a Fountainbleau sandstone [16]. This relation will be applied in the subsequent section.

It should be noted that the approximate formula

$$k = \frac{\Lambda^2}{8F}, \tag{23}$$

developed by Johnson *et al.* [38], provides a good estimate of k for a variety of media. Here Λ^2 is a dynamically weighted ratio of pore volume to surface area that involves the electric field. However, the Λ parameter, to date, has not been experimentally measured.

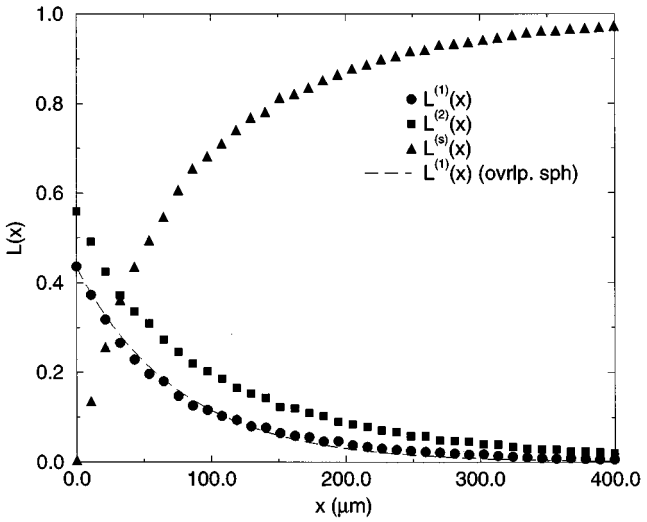

FIG. 3. Lineal-path function $L(i)(x)$ for the void phase, solid phase, and the ''mixed'' phase, in which the random line segment falls in both phases. The result for $L^{(1)}(x)$ in the overlapping sphere system with an equivalent value of ϕ_1 is also shown.

IV. RESULTS

The porosity ϕ_1 of the sample was measured to be 0.44. We note here that the porosity was not constant along the axis of the cylinder, but fluctuated appreciably, indicating the presence of inhomogeneities in the sample. We have chosen to use these formulas defined for homogeneous media since there is no comprehensive theory to account for the inhomogeneities and because the overall structure did still show a significant amount of homogeneity. The specific surface s was also measured and found to be 0.033 $\mu\mathrm{m}^{-1}$. It should be noted that, in general, the specific surface of a digitized image of real material is smaller than the actual specific surface of the material. This is due to the roughness of the surface at length scales smaller than that of the digitization process. This differs from the case of the digitization of an object with a smooth surface, such as a sphere, in which the specific surface of the digitized image is larger than the specific surface of the original object.

In Fig. 3 the lineal-path function is shown for both the void phase and solid phase, along with the probability that a line segment of length x falls in both phases $L^{(s)}(x)$. These three plots must add to unity for all x. The void result is compared to the result for an overlapping sphere system with a similar volume fraction. The radius R of the spheres in the overlapping sphere system was determined by fitting the data to the analytical result for the overlapping sphere system, with the constraint that the volume fraction remains the same. This gives a value of $R=47.3$ μm. The fit also shows the difference between $L^{(1)}(x)$ in the gel and the void phase in the overlapping sphere system. We can see that the gel system decays faster for small z, so there are fewer short-range correlations. For large x, $L^{(1)}(x)$ is larger for the gel system, indicating that there are more larger voids in the gel system than in the overlapping sphere system. Using the data for $L^{(i)}(x)$, we can calculate a value of $\lambda_A^{(1)}=53.8$ μm and $\lambda_A^{(2)}=76.5$ μm.

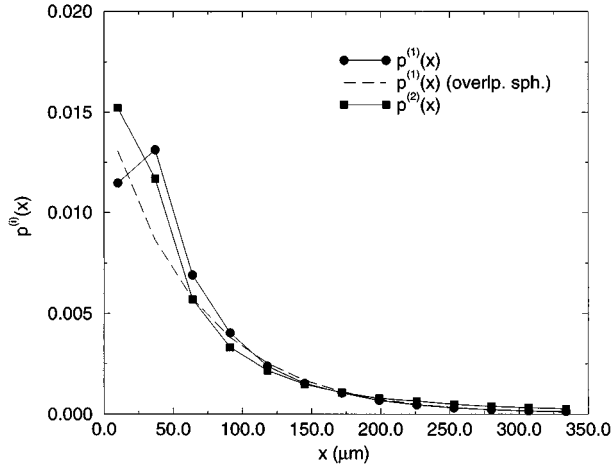

FIG. 4. Chord-length distribution functions $p^{(i)}(x)$ for the two phases of the magnetic gel.

The measurement of $p^{(i)}(x)$ was a bit trickier, due to the digitized nature of the media. The bin widths had to be kept significantly larger due to the noise associated with the chords crossing diagonally across a series of voxels and creating a large number of small chords whose origin is simply an artifact of the digitization. The result is shown in Fig. 4 for the distribution in both the void and gel phase. The distributions are quite similar, unlike the lineal-path functions, mostly because they both must be normalized to unity. Still, the similarity in the two phases is striking, given that they have somewhat different volume fractions. Integrating x times $p^{(i)}(x)$ to get the first moment of each distribution, we get a value of $\lambda_C^{(1)}=67.4$ μm and $\lambda_C^{(2)}=67.9$ μm.

The pore-size distribution $P^{(i)}(x)$ for both phases is presented in Fig. 5 as a function of x. One must take care in interpreting the results displayed in this graph. This is not a

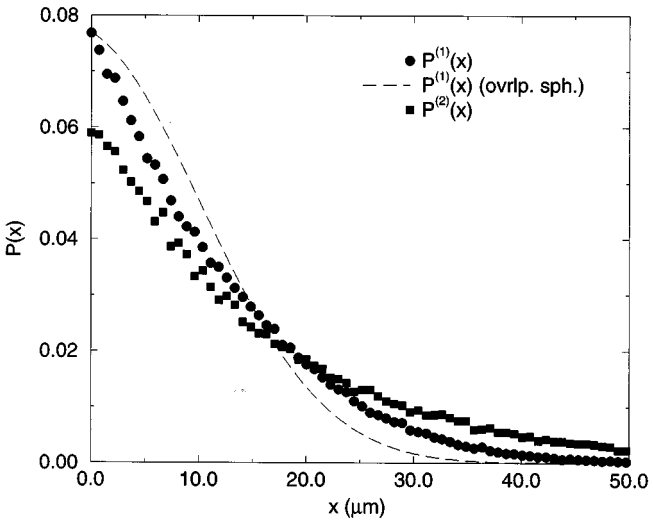

FIG. 5. Pore-size distribution $P^{(i)}(x)$ as a function of x for the magnetic gel sample. The pore-size distribution for the void phase of the overlapping sphere system is shown. The overlapping sphere system was chosen with an equivalent value of $P^{(1)}(0)$ corresponding to an equivalent value of s/ϕ_1.

distribution of the widths of an average pore in the system, but instead a distribution of how far a random spot in phase i in the system is from the nearest wall. To emphasize how these are different, consider two spherical holes in the system of radius R_1 and R_2, where $R_1<R_2$. The random points in R_1 will only contribute to $P^{(1)}(x)$ for small values of x. The random points for R_2 will contribute for larger values of x, but they also contribute to the smaller values of x and, in fact, they make a larger contribution to those smaller values of x due to the fact that the ''volume'' of the spherical shell, which is a distance x away from the nearest wall, will be larger. Calculating the first moment of the distributions of $P^{(i)}$ above, we obtain a value of $\lambda_D^{(1)}=10.7$ μm and $\lambda_D^{(2)}=15.7$ μm. We can check the accuracy of our measurement by noting that $P^{(1)}(0)\phi_1$ gives a value close to the value of the specific surface s.

A plot of the pore-size distribution for an overlapping sphere system is shown in Fig. 5 along with the real physical system. The theoretical curve was chosen to have the same value of $P^{(1)}(0)$ as the gel system, corresponding to having an equivalent value of the ratio of the specific surface to the void volume fraction. Specifying the specific surface automatically determines the radius of the spheres in the overlapping sphere system, which in this case is 32.0 μm. The plot for the theoretical system differs from that of the experimental system in that it is weighted more heavily towards smaller values of x. This shows that the gel system has a broader distribution of pore sizes than the theoretical system. This is similar to what is seen in the plot of $L^{(1)}(x)$.

The numerical value of the mean survival time τ was calculated using the *first-passage cube* algorithm discussed in [39]. Specifically, we found $\tau D\approx 242.6$ μm^2. There is significant variation in the numerical value of τ down the length of the sample. This was partially due to the variation in ϕ_1, as was seen by the correlation between ϕ_1 and τD as a function of slice, and partially due to the variability of the structure along the length of the sample.

Let us now consider estimating the effective transport properties of the gel. The average value of τD is ≈ 242.6 μm^2. It is interesting to compare this value to the rigorous lower bound (18). Since $\lambda_D^{(1)2}=114.5$ μm^2, it is found that τD must be greater than 114.5 μm^2. The ratio of the calculated value of τD to the bound is ≈ 2. Although this bound is not as tight as one would like, this is very close to the ratio in the overlapping sphere system, where the same ratio at $\phi_1=0.44$ is 1.68 [10], indicating that the degree of inhomogeneity in the system does not affect the bound that much.

Now consider estimating the fluid permeability k using cross-property relation (22). In addition to our measured porosity $\phi_1=0.44$ and mean survival time $\tau\approx 242.6$ μm$^2/D$, we need to estimate the formation factor $F=(\sigma_e/\sigma_1)^{-1}$. Following Ref. [18], we shall do this by obtaining a rigorous upper bound estimate of $F^{-1}=\sigma_e/\sigma_1$. Here we use the well-known Hashin-Shtrikman upper bound

$$\frac{\sigma_e}{\sigma_1}\leqslant\frac{\phi_1}{1+\phi_2/2}=0.344. \tag{24}$$

Application of relation (22) yields

$$k\approx 83.5\ \mu\text{m}^2. \tag{25}$$

Note that this permeability estimate is close in value to the square of the mean pore size $\lambda_D^{(1)2}=114.5\mu$m^2.

V. CONCLUSIONS

X-ray microtomographic techniques have enabled us to image in three dimensions the complex connected pore space of a porous magnetic gel. We studied three statistical measures that to some degree reflected connectedness information about the pore and solid phases. In particular, the pore-size distribution, an intrinsically three-dimensional measure, enabled us to bound the trapping rate τ^{-1} of the gel. Moreover, a direct simulation of τ and bound on the formation factor F enabled us to estimate the fluid permeability k using cross-property relations. Estimating the transport properties in this noninvasive fashion is especially useful if the sample is too small or fragile to be characterized using standard experimental procedures, as was the case in our gel sample.

ACKNOWLEDGMENTS

The work at Princeton was supported in part by the MRSEC Program of the National Science Foundation under Contract No. DMR-9400362 and by the U.S. Department of Energy, Office of Basic Energy Sciences under Grant No. DE-FG02-92ER14275.

[1] M. J. Beran, *Statistical Continuum Theories* (Wiley, New York, 1968).
[2] G. W. Milton, Commun. Math. Phys. **111**, 281 (1987).
[3] S. Torquato, Appl. Mech. Rev. **44**, 37 (1991).
[4] S. Prager, Phys. Fluids **4**, 1477 (1961); J. Chem. Phys. **50**, 4305 (1969).
[5] M. Doi, J. Phys. Soc. Jpn. **40**, 567 (1976).
[6] G. W. Milton, Phys. Rev. Lett. **46**, 542 (1981).
[7] J. G. Berryman and G. W. Milton, J. Chem. Phys. **83**, 754 (1985).
[8] J. Rubinstein and S. Torquato, J. Chem. Phys. **88**, 6372 (1988); S. Torquato and J. Rubinstein, *ibid.* **90**, 1644 (1989).
[9] J. Rubinstein and S. Torquato, J. Fluid Mech. **206**, 25 (1989).
[10] S. Torquato and M. Avellaneda, J. Chem. Phys. **95**, 6477 (1991).
[11] S. L. Flegler, *Scanning and Transmission Electron Microscopy: An Introduction* (Freeman, New York, 1993).
[12] *Scanning Tunneling Microscopy*, edited by J. A. Stroscio and W. J. Kaiser (Academic, Boston, 1992).

[13] J. H. Kinney and M. C. Nichols, Annu. Rev. Mater. Sci. **22**, 121 (1992).
[14] J. T. Fredrich, B. Menendez, and T. F. Wong, Science **268**, 276 (1995).
[15] L. M. Schwartz, F. Auzerais, J. Dunsmuir, N. Martys, D. P. Bentz, and S. Torquato, Physica A **207**, 28 (1994).
[16] D. A. Coker, S. Torquato, and J. Dunsmuir, J. Geophys. Res. (to be published).
[17] Y.-N. Jun, D. M. Dabbs, I. A. Aksay, and S. Erramilli, Langmuir **10**, 3377 (1994).
[18] B. Sonuparlak and I. A. Aksay, U.S. Patent No. 4,777,153 (October 1988).
[19] H. W. Deckman, K. L. D'Amico, J. H. Dunsmuir, B. P. Flannery, and S. M. Gruner, Adv. X-Ray Anal. **32**, 641 (1989).
[20] J. H. Dunsmuir, S. R. Ferguson, and K. L. D'Amico, in *Proceedings of the 10th Sympsium on Photoelectric Image Devices, London, 1991*, edited by B. L. Morgan (Institute of Physics, Philadelphia, 1992).
[21] B. P. Flannery, H. W. Deckman, W. G. Roberge, and K. L. D'Amico, Science **237**, 1439 (1987).
[22] H. W. Deckman, J. H. Dunsmuir, K. L. D'Amico, S. R. Ferguson, and B. P. Flannery, in *Advanced Tomographic Imaging Methods for the Analysis of Materials*, edited by J. L. Ackerman and W. A. Ellinqson, MRS Symposia Proceedings No. 217 (Materials Research Society, Pittsburgh, 1991), pp. 97–110.
[23] S. Torquato and G. Stell, J. Chem. Phys. **77**, 2071 (1982).
[24] J. G. Berryman and S. Blair, J. Appl. Phys. **60**, 1930 (1986).
[25] B. Lu and S. Torquato, Phys. Rev. A **45**, 922 (1992); **45**, 7292 (1992).
[26] S. Torquato, M. D. Rintoul, and I. A. Aksay (unpublished).
[27] S. Torquato and B. Lu, Phys. Rev. E **47**, 2950 (1993).
[28] C. E. Krohn and A. H. Thompson, Phys. Rev. B **33**, 6366 (1986).
[29] W. Strieder and S. Prager, Phys. Fluids **11**, 2544 (1968); F. G. Ho and W. Strieder, J. Chem. Phys. **70**, 5635 (1979).
[30] T. K. Tokunaga, J. Chem. Phys. **82**, 5298 (1985).
[31] S. Torquato, Physica A **207**, 79 (1994).
[32] J. R. Banavar and L. M. Schwartz, Phys. Rev. Lett. **58**, 1411 (1987).
[33] D. J. Wilkinson, D. L. Johnson, and L. M. Schwartz, Phys. Rev. B **44**, 4960 (1991).
[34] S. Torquato, Phys. Rev. Lett. **64**, 2644 (1990).
[35] M. Avellaneda and S. Torquato, Phys. Fluids A **3**, 2529 (1991).
[36] S. Torquato and I. C. Kim, J. Appl. Phys. **72**, 2612 (1992).
[37] L. M. Schwartz, N. Martys, D. P. Bentz, E. J. Garboczi, and S. Torquato, Phys. Rev. E **48**, 4584 (1993).
[38] D. L. Johnson, J. Koplik, and L. M. Schwartz, Phys. Rev. Lett. **57**, 2564 (1986).
[39] D. A. Coker and S. Torquato, J. Appl. Phys. **77**, 955 (1995).